Polymer 49 (2008) 2762–2769

Contents lists available at ScienceDirect

Polymer

journal homepage: www.elsevier.com/locate/polymer

Conformational properties and Rouse dynamics of different dendrimer molecules

Juan J. Freire [a,*], Ana M. Rubio [b]

[a] Departamento de Ciencias y Técnicas Fisicoquímicas, Facultad de Ciencias, Universidad Nacional de Educación a Distancia, Senda del Rey 9, 28040 Madrid, Spain
[b] Departamento de Química Física, Facultad de Ciencias Químicas, Universidad Complutense, 28040 Madrid, Spain

ARTICLE INFO

Article history:
Received 7 February 2008
Received in revised form 11 April 2008
Accepted 14 April 2008
Available online 2 May 2008

Keywords:
Dendrimers
Rouse dynamics
Viscoelasticity

ABSTRACT

A coarse-grained model previously proposed to perform Monte Carlo simulations for several dendrimer molecules with different topologies and chemical compositions in solution is employed now to obtain structural properties, such as the bead density profile, the asphericity and the molecular scattering factor, or form factor. It is also used to study the Rouse dynamics, including Rouse spring forces consistent with the equilibrium averages of distances between connected frictional beads and hydrodynamic interactions (Rouse–Zimm scheme). With this approach, the Rouse relaxation times and the frequency-dependent viscoelastic modulus are calculated. Since hydrodynamic interactions are included in their preaveraged form, the effect of the preaveraging approximation is explicitly discussed. The influence of the different structural and topological dependence on the dendrimer static and dynamic properties is analysed and discussed.

1. Introduction

Dendrimers are peculiar nanomolecules of great interest from both the basic and the applied points of view [1]. Numerical simulations are particularly useful to study the structure and dynamics of dendrimer molecules [2]. Taking into account their chemical structure, these molecules can be related to polymers (they are constituted by similar repeat units), though their smaller size and the more congested disposition of units require more specialized simulation models even for the study of global molecular properties. Although these properties can be obtained for detailed atomistic models by means of Molecular Dynamic simulations [3], the simulations actually require a huge computational effort and the use of more simplified models is recommended. These models can be used in conjunction with more efficient numerical techniques. Brownian Dynamics [4] or Monte Carlo (MC) [5] simulations have been performed for simplified models of dendrimers, giving an idea of their general behavior.

Recently, we have proposed [6] specific coarse-grained models useful to perform MC simulations that are able to reproduce the main differences between the experimental molecular properties of several types of dendrimers. The models consider units, which we will denote here as beads, in all the branching points, and additional units in the middle point between beads. In the simulations, the unit positions are changed by a "single-bead jump" algorithm in which the distances between neighboring units and also between neighboring beads follow realistic distributions. These distributions of distances are obtained from Molecular Dynamic simulations previously performed with an atomistic model for the lowest generations. The MC models include a rigid-spheres potential to avoid overlapping of non-neighboring units, described in terms of a fixed minimum distance, or hard-spheres' diameter, σ. This value is assigned to give the best description of the radius of gyration for all the different generations of each given type of dendrimer, according to the existing experimental data. This way, the particular quality of the solvent is implicitly taken into account for each experimental system. Also, a bead frictional radius, r_f, is needed for the evaluation of hydrodynamic properties. It is assigned to give the best reproduction of the experimental data of the intrinsic viscosity for different generations of each type of dendrimer.

Using this description, we have been able to closely reproduce experimental data for the mean quadratic radius of gyration and intrinsic viscosity of several dendrimers in solution [7]. Namely, we have mimicked the properties of polyamidoamine dendrimers with an ethylendiamine core (PAMAM–EDA) and polypropyleneimide with a diaminobutane core (PPI–DAB) in water. We have also reproduced the experimental data of mono-dendrons and tri-dendrons of polybenzylether (mono-PBzE and tri-PBzE) in tetrahydrofuran, THF. Due to the remarkable rigidity of the spacers, or segments between branching points, the best description of the PBzE molecules also requires to take into account the distribution of

* Corresponding author. Tel./fax: +34 3988627.
E-mail address: jfreire@invi.uned.es (J.J. Freire).

0032-3861/$ – see front matter © 2008 Elsevier Ltd. All rights reserved.
doi:10.1016/j.polymer.2008.04.024

angles formed by successive beads [7]. This distribution is similarly obtained from short preliminary Molecular Dynamic runs.

The apparent agreement of our models with the available global properties of these dendrimers in solution has induced us to report results for other interesting properties that may be able to give important differences related with the distinct short range structures and topologies. In particular, we have studied molecular bead density profiles, averaged shapes, characterized by asphericity values, and molecular scattering functions (or form factors). Moreover, we have investigated the Rouse dynamics [8], evaluating the relaxation times and the frequency-dependent viscoelastic moduli. With this end, we have used a modified version of the Rouse theory in which the spring constants corresponding to the connections between pairs of frictional beads are modified to be consistent with their averaged internal distances. A similar scheme was previously applied for linear and star chains with excluded volume interactions [9]. Since these calculations consider hydrodynamic interactions that are implemented in the preaveraged form, the influence of the preaveraging approximation is also discussed.

2. Computational methods

The particular topology of the investigated dendrimers, together with the definition of the generation numbers, the number of beads associated with them and other details of the models used for their MC study were provided in previous work [6,7].

Our statistical samples are constituted by 20 000 configurations obtained from MC trajectories composed of 200×10^6 MC steps for the coarse-grained models described in the preceding section for the different dendrimers. Similar samples have been previously employed [6,7] to evaluate the radius of gyration and the intrinsic viscosity. The latter property was evaluated using the variational Fixman method [10], which usually provides an accurate lower bound. This method includes the consideration of real (i.e. configurationally fluctuating) hydrodynamic interactions. Furthermore, we added a correction term in order to take into account the finite viscosity of single beads [7,11]. The final results for the intrinsic viscosity, $[\eta]_{\text{total}}$, are summarized in Fig. 1 and, as stated in Section 1, show an excellent agreement with most of the available experimental data in solution [7].

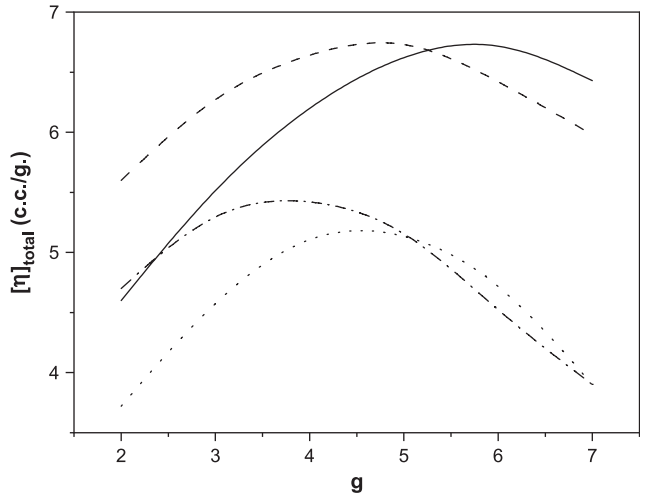

Fig. 1. Summary of the final results for the intrinsic viscosity, $[\eta]_{\text{total}}$, obtained with the coarse-grained models for different dendrimers described in the text. Solid line: PAMAM–EDA, $\sigma = 5.8$ Å, $r_f = 2.65$ Å; dashed line: PPI–DAB, $\sigma = 4.0$ Å, $r_f = 2.65$ Å; dotted line: mono-dendrons of PBzE, $\sigma = 0.5$ Å, $r_f = 2.6$ Å; dash–dotted line: tri-dendrons of PBzE, $\sigma = 0.5$ Å, $r_f = 2.8$ Å. All data include the single-bead correction [7]. The PBzE models include realistic distribution of bead angles [7]. Further details of the models can be found in Refs. [6,7].

The asphericity of a molecule composed of N identical beads can be estimated as [12]

$$A = \frac{\left\langle \sum_{i>j}^{3} (\lambda_i - \lambda_j)^2 \right\rangle}{\left\langle 2\left(\sum_{i=1}^{3} \lambda_i \right)^2 \right\rangle} \tag{1}$$

where λ_k is an eigenvalue of the 3×3 matrix $\langle \mathbf{S}^2 \rangle$, representing the tensor of mean quadratic components of the radius of gyration, obtained form the bead positions.

If the beads are considered also as scattering units, the orientationally and conformationally averaged molecular scattering factor (or form factor) is given by

$$P(q) = N^{-2} \left\langle \sum_i \sum_j \sin(qR_{ij})/qR_{ij} \right\rangle \tag{2}$$

where q is the scattering variable and R_{ij} is the distance between a pair of beads. $\langle\ \rangle$ denotes the conformational average that is performed over the sample of configurations included in an MC trajectory. $P(q)$ results for PAMAM–EDA were anticipated in our previous work [6] and we report them here only for comparison with those obtained for the other molecules.

The Rouse theory [8,13] gives a standard description of the dynamic properties of chain molecules, though it is only rigorously valid to describe the dynamics of Gaussian polymer chains. It uses the representation of a molecule by friction points, assimilated here to our model beads, which are connected by elastic springs. The Rouse theory can give an approximate description of molecules whose internal distances do not follow a Gaussian distribution, assuming that they are similarly connected by springs with consistent spring constants. This way, the molecular dynamics can still be described in terms of $N - 1$ normal mode coordinates, $\mathbf{U}_k$, relaxing as e^{-t/τ_k} (τ_k is defined as the kth relaxation time). This assumption should be consistent with the general approximate expression for the potential energy [8]

$$U/k_B T = \frac{1}{2} \sum_{k=1}^{N-1} 3\mathbf{U}_k^2 / \langle \mathbf{U}_k^2 \rangle \tag{3}$$

The treatment applied in this work also considers preaveraged hydrodynamic interactions, following the theoretical approach proposed by Zimm [14]. These interactions are described by a modified (Rotne–Prager–Yamakawa) version of the Oseen tensor [15]. They are introduced in the $N \times N$ hydrodynamic interaction matrix, $\mathbf{H}$,

$$H_{ii} = 1$$

and

$$H_{ij} = \operatorname{erf}(x) - \frac{1 - e^{-x^2}}{\pi^{1/2} x}, \quad i \neq j \tag{4}$$

with

$$x = (\xi / 6\pi\eta_0) \left\langle R_{ij}^{-1} \right\rangle \tag{5}$$

where $\langle R_{ij}^{-1} \rangle$ is the mean reciprocal distance between beads i and j. The bead friction coefficient, $\xi = 6\pi\eta_0 r_f$, depends on the solvent viscosity, η_0, and the bead friction radius. We have employed here the same values of r_f used to calculate the intrinsic viscosity with the Fixman method, as described in the caption of Fig. 1.

It has been shown [9] that Eq. (3) and the consideration of hydrodynamic interactions allow for the calculation of the reduced relaxation times, $(\tau_k)^* = (6k_B T/\xi b^2)\tau_k$, where $k_B T$ is the Boltzmann

factor and b is the mean segment length, according to the following formula:

$$(\tau_k)^* = \nu_k^{-1}\langle \mathbf{U}_k^2\rangle/b^2, \quad k = 1, N-1 \tag{6}$$

ν_k^{-1} is the kth eigenvalue of matrix $\mathbf{H}^{-1}$. The $N-1$ elements $\langle \mathbf{U}_k^2\rangle$, representing the mean quadratic length of the k normal coordinate, are obtained as

$$\langle \mathbf{U}_k^2\rangle = \sum_{i=1}^{N}\sum_{j=1}^{N}\left(\mathbf{Q}^{-1}\right)_{ki}\langle \mathbf{R}_i\cdot\mathbf{R}_j\rangle\left(\mathbf{Q}^{-1}\right)_{kj}, \quad k = 1, N-1 \tag{7}$$

where $\mathbf{Q}$ is an orthogonal matrix, containing the eigenvectors of the product matrix $\mathbf{HA}$ (whose N eigenvalue is zero) and $\mathbf{R}_i$ is the position of bead i referred to a viscosity center that is usually approximated by the center of masses of the molecule. The averages $\langle \mathrm{R}_i\cdot\mathrm{R}_j\rangle$ can actually be obtained from the mean quadratic averages of distances between beads, $\langle R_{ij}^2\rangle$. Finally, $N\times N$ matrix $\mathbf{A}$ is defined from the topology of the spring connections between the beads,

$$A_{ii} = n_{\mathrm{con}},$$

where n_{con} is the number of springs directly connecting bead i with neighboring beads,

$$A_{ij} = -1$$

for $i \neq j$ and connected, and

$$A_{ij} = 0 \tag{8}$$

for $i \neq j$ and non-connected.

With this formulation, we can also evaluate the complex viscoelastic modulus, $[G(\omega)]\equiv i\omega\eta_0[\eta(\omega)]$, related to the frequency-dependent viscosity, $[\eta(\omega)]$. In its reduced version, $[\eta(\omega)]^*$, the latter property can easily be evaluated from the reduced relaxation times,

$$[\eta(\omega)]^* \equiv \frac{6M\eta_0}{N_A\xi b^2}[\eta(\omega)] = \sum_{k=1}^{N}\frac{(\tau_k)^*}{1+i\omega^*(\tau_k)^*} \tag{9}$$

where M is the molecular weight, proportional to the number of beads, N_A is the Avogadro number and $\omega^* = (\xi b^2/6k_BT)\omega$. Similarly, the reduced complex viscoelastic modulus is defined as $[G(\omega)]^*\equiv(M/RT)[G(\omega)]$ and its components are calculated as

$$\left[G'(\omega)\right]^* = \sum_{k=1}^{N-1}\frac{\left[\omega^*(\tau_k)^*\right]^2}{1+\left[\omega^*(\tau_k)^*\right]^2},$$

$$\left[G''(\omega)\right]^* = \sum_{k=1}^{N-1}\frac{\omega^*(\tau_k)^*}{1+\left[\omega^*(\tau_k)^*\right]^2} \tag{10}$$

Therefore, we can obtain $[G(\omega)]^*$ if we calculate the different averages $\langle R_{ij}^{-1}\rangle$ and $\langle R_{ij}^2\rangle$ from our MC conformational sample. The validity of this scheme for molecules with non-Gaussian distributions of internal distances was successfully tested by comparison with numerical results obtained with Brownian Dynamic simulations (consistently using preaveraged hydrodynamic interactions) for linear and star polymer chains with excluding volume interactions [9].

3. Structural properties

Table 1 summarizes the estimated asphericities and densities for the different dendrimers. Reference values [12] are $A = 0.526$ for ideal (Gaussian) linear polymers and $A = 0.183$ for a 6-arms' star polymer, together with the obvious result $A = 0$ for spheres. Most of the data show the expected decrease of asphericity, implying a more globular shape, when the generation number, g, is increased. This effect is related with the increase of compactness due to a higher congestion of units. Since all asphericity values are relatively low, we have estimated the mean density of dendrimer mass within the molecules (or bead density in mass) assuming that the molecules are spheres

Table 1
Asphericities and bead densities (in g/cc) for different dendrimers

Molecule	g	A	ρ
PAMAM–EDA	3	0.053	0.35
	4	0.027	0.32
	5	0.015	0.34
	6	0.009	0.36
	7	0.11	0.38
PPI–DAB	3	0.078	0.44
	4	0.045	0.43
	5	0.027	0.46
	6	0.016	0.48
	7	0.111	0.56
Mono-dendron PBzE	3	0.24	0.35
	4	0.16	0.36
	5	0.11	0.42
	6	0.08	0.54
	7	0.06	0.77
Tri-dendron PBzE	3	0.18	0.37
	4	0.13	0.41
	5	0.09	0.51
	6	0.08	0.67
	7	0.37	0.95

$$\rho = M/(4\pi/3)\left[(5/3)R_g^2\right]^{3/2}N_A \tag{11}$$

where R_g^2 is the mean quadratic radius of gyration. Only the more flexible PAMAM–EDA and PPI–DAB dendrimers show a minimum in bead density. Even in these cases, the minimum is not clearly marked. Moreover the assumption of spherical form and the statistical errors of about 3% in the density data (based on errors of about 1% for our previous estimations of the radius of gyration) can lead to real uncertainties greater than the differences between these particular data. The PBzE molecules with short and rigid spacers show a monotonous increase in density that becomes very remarkable for the highest generation numbers. For our highest dendrimer generation, $g = 7$, bead density is clearly correlated with the extension and flexibility of the spacer segments between branching points. Thus, the PAMAM–EDA dendrimers with longer flexible spacers are clearly less dense than the PPI–DAB molecules, while the mono-PBzE dendrimers are denser. The more congested tri-PBzE molecules reach even higher bead densities close to the melt value.

In Table 1, it is observed that there is also a correlation between spacer flexibility and asphericity. The PBzE molecules, with more rigid spacers, exhibit higher asphericities for similar generation number than the more flexible PAMAM–EDA and PPI–DAB molecules. Moreover, PPI–DAB dendrimers show a higher asphericity than the homologous PAMAM–EDA, with longer and more flexible spacers. It seems that, when comparing molecules of different types, this is the relevant effect and differences in densities are not mainly determining the dendrimer shapes. However, when comparing the lowest generations of PBzE mono-dendrons and tri-dendrons, both with the same rigid spacers, it is observed that congestion of units in the tri-dendrons tends to decrease asphericity as the bead density increases. It should also be noted that abnormal values of the asphericity are obtained for the highest generation number, $g = 7$. We observe a noticeable increase in asphericity, not related with any remarkable change in other properties, except in the case of the mono-PBzE molecules. A

similar great asphericity increase has been reported in Molecular Dynamic simulations [3] performed for PAMAM–EDA. Also, Timoshenko et al. reported a minimum in the asphericity at intermediate generation numbers in their Monte Carlo study of a generic model for co-dendrimers [16], defined with different interaction (Lennard-Jones) parameters for the external and internal units. (In their previous study of dendrimers composed of a single type of units, however, the asphericity showed a monotonous decrease with generation number [17].) The minimum suggests that a shape change is needed to accommodate new repeating units when the number of branches reaches a large value, due to strong steric interactions between congested units in the outer generation shell of the molecules.

In Figs. 2 and 3, we have represented generalized Kratky plots [18], $x^{5/6}P(x)$ vs $x^{1/2}$, with $x = q^2R_g^2$, corresponding to the form factors for the different dendrimer molecules with generation numbers 5 and 7. These plots underline the main features of the different systems. (Exponent 5/6 is consistent with assuming that the dendrimers are immersed in a good quality solvent and they show excluded volume effects at least in the short distance range.) We compare our results with the theoretical result for a compact sphere. We also include the form factor corresponding to a linear chain with excluded volume [19]. The sphere plot shows an oscillatory behavior with many peaks that decrease in intensity as x increases. It is noticed that all the systems show behaviors very different from the linear chain curve and clearly tend to mimic the sphere sharp maximum, indicating a significantly compact structure. Moreover, the PAMAM–EDA and PPI–DAB dendrimer plots reproduce the smaller secondary peak of the sphere, both in position and in intensity for $g = 7$. Furthermore, the position of the sphere's third peak is also suggested. In the $g = 5$ case, these dendrimers show a good reproduction of the main maximum and exhibit a second peak whose position is also in agreement with the sphere model. This implies that the inner structure of the dendrimers is very close to a compact sphere for $g = 7$ and it is close to this model even for the $g = 5$ molecules that have smaller densities of beads. We should also note that a satisfactory comparison between our results for PAMAM–EDA and some experimental data [20] for the $g = 5$ in methanol was performed in previous work [6].

However, the PBzE molecules show less homogeneous structures, in spite of their higher densities. Although the first maximum is again closely reproduced, the values are higher than the sphere

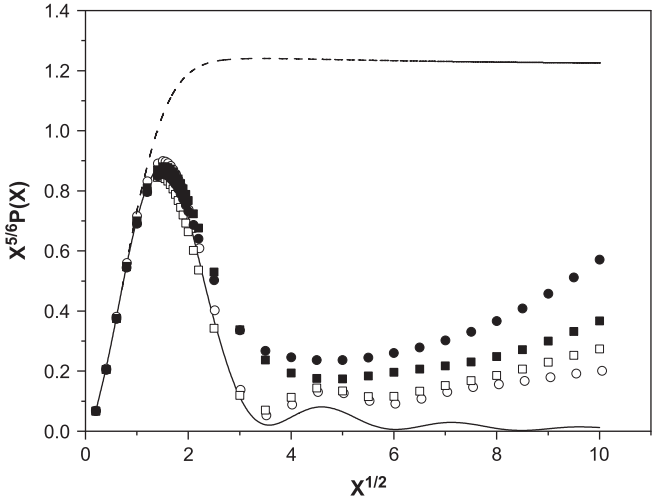

Fig. 2. Generalized Kratky plot of the form factor obtained with the coarse-grained models for different dendrimers with $g = 5$. Open circles, PAMAM–EDA; open squares: PPI–DAB; closed circles: mono-dendrons of PBzE; closed squares: tri-dendrons of PBzE; solid line: compact sphere; dashed line: linear polymer coil with excluded volume interactions [17].

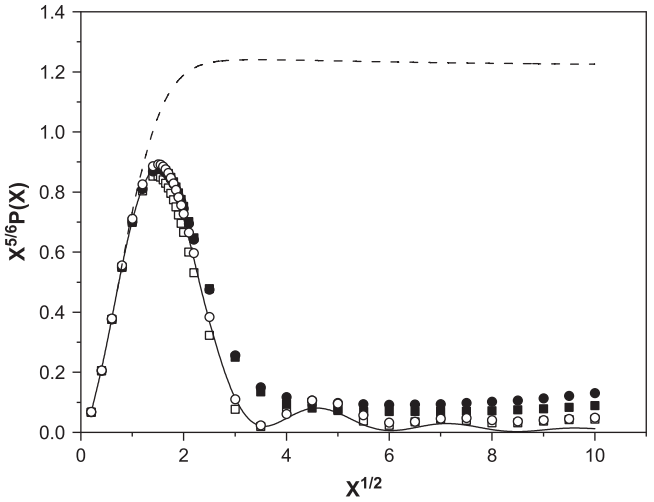

Fig. 3. Generalized Kratky plot of the form factor obtained with the coarse-grained models for different dendrimers with $g = 7$. Open circles: PAMAM–EDA; open squares: PPI–DAB; closed circles: mono-dendrons of PBzE; closed squares: tri-dendrons of PBzE; solid line: compact sphere; dashed line: linear polymer coil with excluded volume interactions [17].

results beyond the maximum position and there is not any indication of secondary peaks. This tendency also correlates to the remarkable higher asphericities shown by the PBzE molecules, discussed above, and it is more marked for the less dense mono-dendrons. For $g = 5$ (molecule with smaller radius of gyration, i.e. with a greater q for a given value of x in the graphic) the results tend to increase more abruptly for $x > 4$, indicating that the monitored distances are within the coarse-grained beads in this x range. Some small-angle neutron scattering experimental data of mono-PBzE ($g = 3$–5) in deuterated THF have been reported [21] and their standard, $q^2P(x)$ vs x, Kratky plots show a very pronounced maximum and no further evidence of structure for higher q. Although the significant statistical noise of the data in the q-high region hinders a precise comparison, it looks that the plateau in this region always lies considerably higher than the sphere oscillations, in qualitative agreement with the present results.

In Fig. 4 we show the bead density profiles $\rho(R_c)$ (R_c is the distance between beads and the center of masses) corresponding to the different dendrimers with $g = 5$. In Fig. 5 we have also plotted

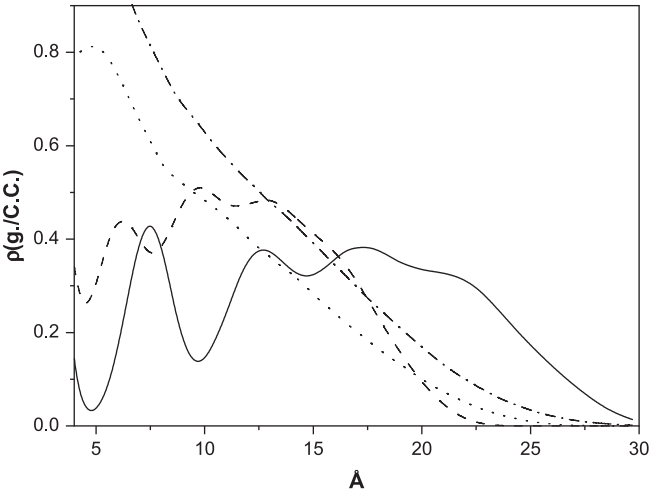

Fig. 4. Total bead density profiles (in mass) obtained with the coarse-grained models for different dendrimers with $g = 5$. Solid line: PAMAM–EDA; dashed line: PPI–DAB; dotted line: mono-dendrons of PBzE; dash–dotted line: tri-dendrons of PBzE.

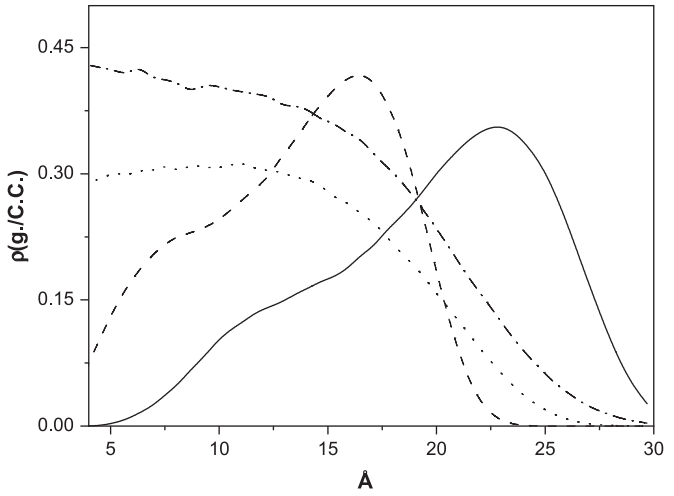

Fig. 5. Normalized outer shell bead density profiles (in mass), $(N/N_{out})\rho_{out}(R_c)$, obtained with the coarse-grained models for different dendrimers with $g = 5$. Solid line: PAMAM–EDA; dashed line: PPI–DAB; dotted line: mono-dendrons of PBzE; dash–dotted line: tri-dendrons of PBzE.

$\rho_{out}(R_c)$, where subscript out denotes beads belonging to the outer generation shell. (This density is appropriately normalized to perform direct quantitative comparisons with the total bead density values.) PAMAM-EDA and PPI–DAB show a typical shell structure, with bead densities showing several peaks of similar heights at various distances in the inner core. Furthermore, it can be observed that the peaks are wider in PAMAM–EDA, due to the larger extension of its spacers and the higher value of the overlapping distance parameter σ. The outer shell bead densities have a clear maximum for high values of R_c, indicating that the end beads are mainly located in the external part of the molecules. This is in agreement with MD simulations trying to mimick PAMAM–EDA molecules in low or medium pH solutions [3]. (This experimental conditions also correspond to the radius of gyration data reproduced by the present simulations).

However, the mono-dendrons and tri-dendrons of PBzE show important qualitative differences from this scheme. Their total bead densities decrease in much of the range of values of R_c, indicating less homogeneous structures, in agreement with the conclusion obtained from the Kratky plots. Moreover, although the normalized value of the outer shell densities is clearly higher than the total density at high R_c, the $\rho_{out}(R_c)$ profiles are constant or slightly decreasing in the molecule core, which indicates a more important backfolding of the end beads. This behavior is typical of denser, though not necessarily more homogeneous, structures. For instance, the MD simulations of PAMAM–EDA in high pH solutions show total bead density profiles with a prominent peak followed by a decrease near the core and secondary peaks [3]. From the theoretical point of view, it can be argued that denser dendrimers follow more closely the decreasing density behavior predicted by Boris and Rubinstein self-consistent field calculations [22], while less dense dendrimers are more likely to be organized in shells. In the particular case of the PBzE molecules, the density profile decrease is associated with the changes in the parameter values and the introduction of further structural details that are needed for a better reproduction of the global experimental data of radius of gyration and viscosity [7].

3.1. Rouse dynamics

The dendrimer dynamics can be understood through its description in terms of Rouse modes and relaxation times, including hydrodynamic interactions. We should remark that the Rouse dynamics of dendrimers composed by Gaussian springs without hydrodynamic interactions have been previously reported [23]. Moreover, the dynamics of a general freely jointed model of dendrimers with preaveraged hydrodynamic interactions have also been investigated [24]. A similar study has been performed considering excluded volume interactions through a self-consistent minimization of the intramolecular free energy [25]. This minimization takes into account the deviations with respect to the dynamic description based on Gaussian springs. As described in the preceding section, our calculations include the description of realistic distributions of bond distances and angles and also of interactions between non-bonded beads.

Table 2
Reduced first Rouse relaxation time for different dendrimers

Molecule	g	$(\tau_1)^*$
PAMAM–EDA	3	135
	5	649
	7	3380
PPI–DAB	3	72.8
	5	303
	7	1200
Mono-dendron PBzE	3	91.9
	5	321
	7	792
Tri-dendron PBzE	3	109
	5	339
	7	865

Our results for the reduced first (highest) Rouse relaxation times corresponding to some of the different dendrimers according to our coarse-grained model are shown in Table 2. The variation of these values with the generation number for a given type of dendrimer is mainly related with the increase of the number of beads and molecular volume. Comparing different dendrimers with similar N, higher relaxation times correspond to lower bead densities, remarking their main dependence on the global molecule size. A slower growth of the molecule size with g, associated with the remarkable increase in density, explains why we observe smaller differences in the values of $(\tau_1)^*$ for increasing values of g in the case of PBzE molecules.

In Fig. 6 we plot τ_k/τ_1 for the different molecules with $g = 7$ and perform a comparison with the values provided by the Rouse–Zimm scheme [26], $\tau_k \approx [k^{3/2}(1 - 1/2\pi k)]$ for an ideal linear polymer (Gaussian coil) in the non-draining limit. It can be observed

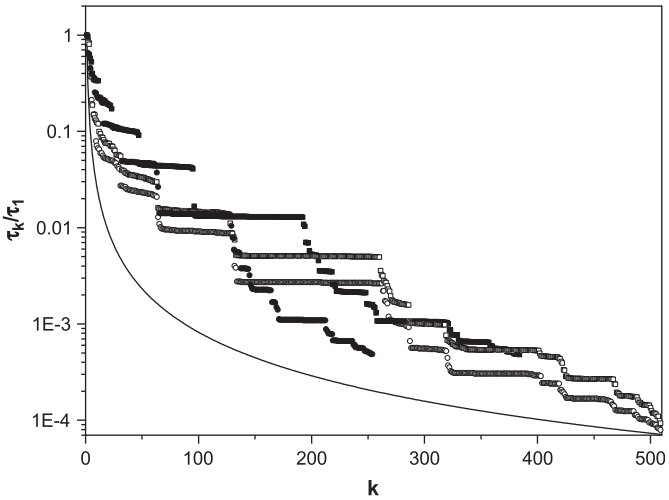

Fig. 6. τ_k/τ_1 obtained with the coarse-grained models for different dendrimers with $g = 7$. Open circles: PAMAM–EDA; open squares: PPI–DAB; closed circles: mono-dendrons of PBzE; closed squares: tri-dendrons of PBzE. Solid line: Results for an ideal linear polymer (Gaussian coil) in the non-draining limit.

that the relaxation time spectra of the dendrimers are significantly different from the linear polymer chain. The dendrimer data show a remarkable slower variation with k and many degenerate (or close-to-degenerate) values are associated to the different types of branching points, as also shown in previous studies with generic dendrimer models [23–25]. The higher values of τ_k/τ_1 obtained for the long and intermediate relaxation times of the dendrimers imply higher viscoelasticity for dendrimer molecules than for linear polymer chains of equivalent size and density, due to the presence of many branching points. Also, there are important differences between the results obtained for the tri-dendron of PBzE, with a higher bead density and more rigid spacers, and the PAMAM–EDA or PPI–DAB dendrimers, with more branching points or beads, but less dense and with flexible spacers. The tri-dendron molecule shows a slow decay with k for low values of k, which is related to its long time behavior due to its higher density and rigidity. This decay, however, significantly increases for higher values of k. PAMAM–EDA shows an initial faster decay but there is a wide plateau of degenerate values for intermediate k, range for which τ_k/τ_1 is actually similar, or even greater, than that in the tri-dendron case. This implies a peculiar dynamics at the transition from long to short times for the PAMAM–EDA molecule, also observed for PPI–DAB. This molecule exhibits values of τ_k/τ_1 slightly higher than those of PAMAM–EDA in the whole range of values of k, due to its greater bead density and more rigid spacers. Less dense mono-dendrons of PBzE show an initial decay close to tri-dendrons, remarking the influence of rigidity in the long time range, but the decay becomes faster at intermediate k as in the tri-dendron case, giving values of τ_k/τ_1 significantly smaller than the rest of molecules.

Figs. 7–9 summarize the log–log variation of the reduced complex viscoelastic modulus with frequency, calculated with the Rouse–Zimm scheme, for the investigated dendrimers. In these plots, frequency is expressed as

$$\omega_R \equiv (M\eta_0[\eta]/RT)\omega = [\eta]^*\omega^* \tag{12}$$

where

$$[\eta]^* \equiv [\eta(\omega = 0)]^* = \sum_{k=1}^{N-1}(\tau_k)^* \tag{13}$$

According to Eqs. (10), (12) and (13), curves representing the imaginary modulus should converge at low frequency showing linear increase with slope equal to 1 so that the precise location of their deviation from linearity when frequency increases can be easily appreciated for the different molecules. The deviation occurs (for both the real and the imaginary moduli) when $\omega^*(\tau_1)^* \cong 1$ or $\omega_R \cong [\eta]^*/(\tau_1)^*$. The real modulus at low frequencies should show a slope equal to 2 for all molecules, with absolute values depending on $\sum_{k=1}^{N-1}[(\tau_k)^*/[\eta]^*]^2$. Ratio $(\tau_k)^*/[\eta]^*$ tends to slowly decrease when N increases, because of the contribution of additional shorter relaxation times to $[\eta]^*$, see Eq. (13). Consequently, higher values of N usually imply smaller values of the real modulus. Moreover, the $(\tau_1)^*/[\eta]^*$ decrease implies that a significant deviation of both moduli from linearity will only be noticed for higher values of ω_R. This also determines the location order of the different imaginary module curves at intermediate frequencies.

Eq. (10) shows that the imaginary modulus curves finally decrease in the high-frequency range, while the real modulus curves approach to an asymptotic limit value, $N-1$. However, it should be also remarked that the present theoretical model is expected to fail at high frequencies unless realistic constraints substitute the spring

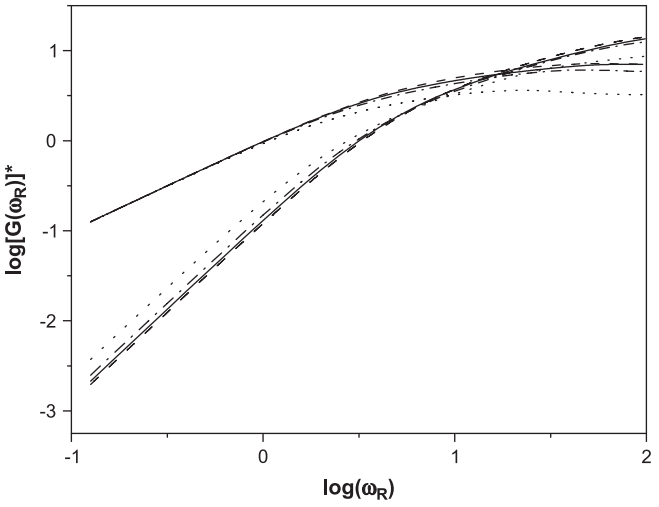

Fig. 8. log–log plots of the real (lower curves on the left side) and imaginary (upper curves on the left side) components of $[G(\omega_R)]^*$ obtained with the coarse-grained models for different dendrimers with $g = 3$. Solid line: PAMAM–EDA; dashed line: PPI–DAB; dotted line: mono-dendrons of PBzE; dash–dotted line: tri-dendrons of PBzE.

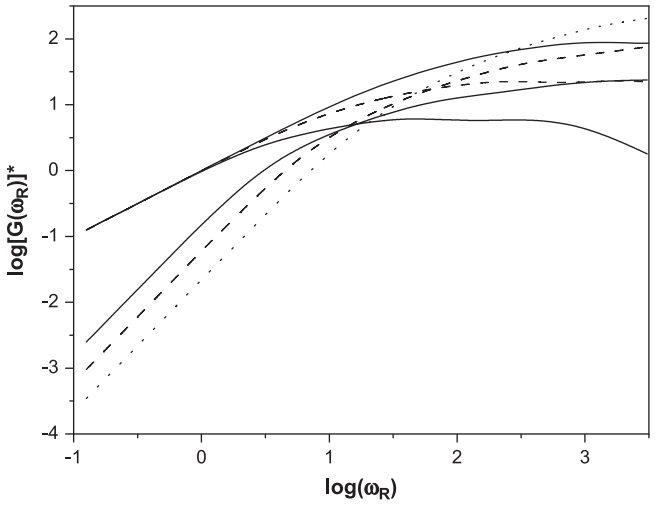

Fig. 7. log–log plots of the real (lower curves on the left side) and imaginary (upper curves on the left side) components of $[G(\omega_R)]^*$ obtained with the coarse-grained model for different generations of PBzE tri-dendrons. Solid line: $g = 3$; dashed line: $g = 5$; dotted line: $g = 7$.

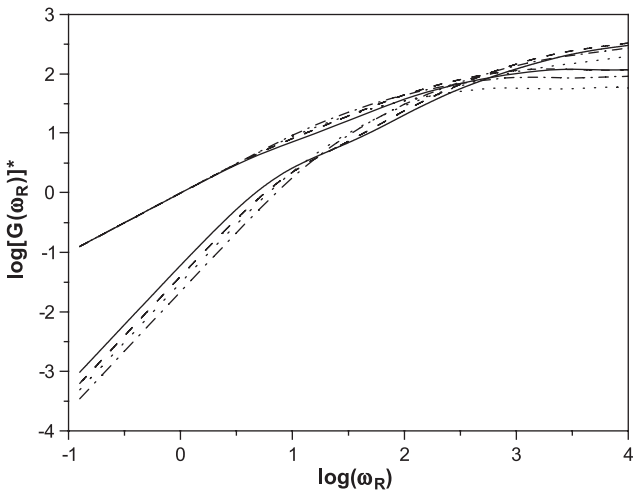

Fig. 9. log–log plots of the real (lower curves on the left side) and imaginary (upper curves on the left side) components of $[G(\omega_R)]^*$ obtained with the coarse-grained models for different dendrimers with $g = 7$. Solid line: PAMAM–EDA; dashed line: PPI–DAB; dotted line: mono-dendrons of PBzE; dash–dotted line: tri-dendrons of PBzE.

constants to describe the molecule in the short time range (rigid connections). These constraints prevent the imaginary (or loss) modulus, $G''(\omega)$, from decreasing. Actually, the high-frequency decrease and the associated plateau for the real (or storage) modulus, $[G'(\omega)]$, are never found in real molecules since they are features associated with the consideration of a finite number of elastic springs [27,28].

Fig. 7 compares the results obtained for the tri-dendrons of PBzE with several generation numbers. It is observed that the increase in g leads to some decrease in the real modulus at low frequencies and to a later departure of the linear behavior for both the real and the imaginary moduli. These features are associated with the increase of N discussed in the preceding paragraph. Consequently, the maximum in the imaginary modules and the curve crossing also appear at higher frequencies, widening the range of validity of the Rouse model. We can also note that the real modulus curves corresponding to different dendrimers should intercept at intermediate frequencies to invert their order and reach their predicted $N-1$ limit values.

Fig. 8 shows the curves for different dendrimers and $g=3$. We can notice similar curves for PAMAM–EDA, PPI–DAB and the PBzE tri-dendron. However, the mono-dendrons of PBzE show a significantly higher value of the real module at low frequencies and also earlier curvature. The peculiar behavior of the PBzE mono-dendrons is surely due to the smaller number of beads, or branching points, of this molecule with respect to the other three cases. PAMAM–EDA and PPI–DAB have the same number of branching points for a given g and the number of beads is slightly higher but close to the value corresponding to the PBzE tri-dendrons for $g=3$. Therefore, the real modulus of the latter molecule lies above the PAMAM–EDA curve at low frequencies. Finally, the real modulus corresponding to PPI–DAB lies slightly below the PAMAM–EDA at low frequencies. It seems that, for similar number of beads, this order is determined inversely to the bead densities. As in the cases shown in Fig. 7, the real modulus curves intercept at intermediate frequencies to invert their order and reach their asymptotic values.

Fig. 9 contains a similar comparison between the different dendrimers for $g=7$. As an obvious difference with the $g=3$ case, it can be observed that the deviation from linearity, $[G'(\omega)]^*$ maximum and curve crossing are located at considerably higher frequencies, because of the increase in the number of beads. For $g=7$, the number of branching points of both mono-dendrons and tri-dendrons of PBzE becomes more similar (though tri-dendrons always have more beads than mono-dendrons for any given g). This explains the approach of the mono-dendron and tri-dendron curves with respect to the $g=3$ case. N is in both cases smaller than that for the PAMAM–EDA and PPI–DAB dendrimers. However, the PAMAM–EDA and PPI–DAB dendrimers show greater values of the real modulus than the PBzE molecules at low frequencies. These low frequency values are now ordered inversely to the different bead densities.

Moreover, the PAMAM–EDA and PPI–DAB dendrimers and the mono-dendrons of PBzE exhibit an earlier deviation from linearity and cross the tri-dendron real modulus curves at intermediate frequencies. The deviation from linearity at higher frequencies and the behavior at intermediate frequencies seem to be mainly conditioned by both the spacer rigidity and the density. The real and imaginary curves corresponding to the less dense and more flexible PAMAM–EDA molecule cross the corresponding PPI–DAB curves in the intermediate frequency range. The curve shapes of the PAMAM–EDA and PPI–DAB dendrimers and, in a lesser extension, of the mono-dendrons of PBzE, somehow resemble the behavior previously reported for highly branched star chains, with an earlier and more extended approach of the real and imaginary parts before they cross [9]. Similar shapes have also been obtained with a general dendrimer model [25]. On the other hand, the more rigid and denser tri-dendrons of PBzE exhibit smoother curves. They are more similar to the curves obtained for low-g dendrimers and also to those previously reported for linear polymer chains [29] and dendrimers with Gaussian spring connections [24], avoiding the earlier deviation from linearity.

Table 3
Ratio between the preaveraged and the correct conformational intrinsic viscosity for different dendrimers

Molecule	g	$[\eta]_{cf}/[\eta]$
PAMAM–EDA	3	0.729
	5	0.644
	7	0.544
PPI–DAB	3	0.766
	5	0.562
	7	0.432
Mono-dendron PBzE	3	0.855
	5	0.594
	7	0.325
Tri-dendron PBzE	3	0.733
	5	0.490
	7	0.257

We should finally discuss the consequences of using of preaveraged hydrodynamic interactions in the Rouse–Zimm scheme. This approximation has been shown to give important quantitative differences in the description of the (zero frequency) intrinsic viscosity with respect to treatments [2,10,30] that include real (fluctuating) hydrodynamic interactions. Since our results for the intrinsic viscosity, shown in Fig. 1, were calculated by using the variational Fixman method where fluctuating hydrodynamic interactions are introduced, we can evaluate the influence of using preaveraged hydrodynamic interactions for the particular dendrimers studied in this work. Table 3 shows the ratio between the zero frequency intrinsic viscosity obtained with fluctuating hydrodynamic interactions (conformational contribution to the intrinsic viscosity; denoted with subscript cf) and with the Rouse–Zimm approach based on the preaveraging approximation (no subscript), $[\eta]_{cf}/[\eta]$, for different dendrimers. It is verified that, from the quantitative point of view, the preaveraging approximation is particularly inaccurate for the dendrimers with higher bead density. This is consistent with our previous results for linear chains and stars [31]. The results showed that preaveraging is a poorer approximation for molecules with high density of beads in the molecule core.

Unfortunately, it is not easy to include fluctuating hydrodynamic interactions in the theoretical scheme to estimate the frequency-dependent viscosity, i.e. the viscoelastic modulus at finite frequencies, from an equilibrium sample. In this case, dynamic simulations are prescribed to obtain a slowly decaying stress time-correlation function [29,32]. Brownian Dynamic simulations have been previously performed for this purpose for linear, star and ring flexible polymers without intramolecular interactions and results for the reduced viscoelastic modulus have been reported [29]. These results showed that the preaveraging approximations have a similar influence for both $[G'(\omega)]$ and $[G''(\omega)]$. It was verified that $[G'(\omega)]_{cf}/[G'(\omega)]$ and $[G''(\omega)]_{cf}/[G''(\omega)]$ practically remain constant in the range of frequency for which both moduli show a linear increase in a log–log plot.

Preaveraged and fluctuating hydrodynamic curves are coincident for high frequencies where the present model is unrealistic, since they yield identical values of the stress correlation function at $t=0$ [32]. Consequently, the preaveraged results actually give a good qualitative description of the dynamic moduli behavior in the range of low and moderate frequencies where the Rouse model is adequate, though important quantitative differences are shown with respect to the real values, and these

differences depend on the particular molecular topology. Deviations from the log–log linear increase occur at lower frequency values when the preaveraging approximation is considered [29]. Nevertheless, the consistent use of preaveraging for different molecules in the present work may help to understand how the topological and structural details also influence these deviations.

Acknowledgements

This work has been partially supported by Grant CTQ2006-06446 from DGI-MEC, Spain.

References

[1] Fréchet JMJ, Tomalia DA, editors. Dendrimers and other dendritic polymers. Chichester (England): Wiley; 2001.
[2] Freire JJ. Adv Polym Sci 1999;143:35.
[3] Maiti PK, Çağin T, Wang GF, Goddard III WA. Macromolecules 2004;37:6236.
[4] Lyulin AV, Davies GR, Adolf DB. Macromolecules 2000;33:3294.
[5] Mansfield ML, Klushin LI. Macromolecules 1996;26:4262.
[6] Freire JJ, Rodríguez E, Rubio AM. J Chem Phys 2005;123:154901.
[7] Rodríguez E, Freire JJ, del Río Echenique G, Hernández Cifre JG, García de la Torre J, Rubio AM. Polymer 2005;48:1155.
[8] Doi M, Edwards SF. The theory of polymer dynamics. Oxford, England: Clarendon, Wiley; 1986.
[9] Rey A, Freire JJ. J Chem Phys 1995;104:758.
[10] Fixman MJ. Chem Phys 1983;78:1588.
[11] García de la Torre J, del Río Echenique G, Ortega A. J Phys Chem B 2007;111:955.
[12] Wei G, Eichinger BE. J Chem Phys 1990;93:1430.
[13] Rouse PE. J Chem Phys 1953;21:1272.
[14] Zimm BH. J Chem Phys 1956;24:269.
[15] Yamakawa H. J Chem Phys 1970;78:1594.
[16] Connolly R, Timoshenko EG, Kuznetsov Yu A. Macromolecules 2004;37:7381.
[17] Timoshenko EG, Kuznetsov Yu A, Connolly R. J Chem Phys 2002;117:9050.
[18] Burchard W. Macromolecules 1997;10:919.
[19] Rubio AM, Álvarez G, Freire JJ. Polymer 2008;49:628.
[20] Prosa TJ, Bauer BJ, Amis EJ, Tomalia DA, Scherrenberg R. J Polym Sci Part B Polym Phys 1997;35:2913.
[21] Tande BM, Wagner NJ, Mackay ME, Hawker CJ, Jeong M. Macromolecules 2001;34:8580.
[22] Boris D, Rubinstein M. Macromolecules 1996;29:7251.
[23] Cai C, Chen ZY. Macromolecules 1997;30:5104.
[24] La Ferla R. J Chem Phys 1997;106:688.
[25] Ganazzoli F, La Ferla R, Raffaini G. Macromolecules 2001;34:4222.
[26] Yamakawa H. Modern theory of polymer solutions. New York: Harper and Row; 1971.
[27] Bird RB, Hassager O, Armstrong RC, Curtiss CF. Dynamics of polymeric liquids. New York: Wiley; 1977.
[28] Fixman M. J Chem Phys 1988;89:2442.
[29] Rey A, Freire JJ, García de la Torre J. J Chem Phys 1990;92:6278.
[30] Zimm BH. Macromolecules 1980;13:592.
[31] Freire JJ, Rey A, Bishop M, Clarke JHR. Macromolecules 1991;24:6494.
[32] Fixman M. J Chem Phys 1983;78:1594.